Journal of Applied Mechanics and Technical Physics, Vol. 43, No. 1, pp. 154–161, 2002

LIMITING DEFORMABILITY AND STRENGTH OF BASALT–PLASTIC SHELLS UNDER INTERNAL EXPLOSIVE LOADING

V. N. Rusak,[1] A. G. Fedorenko,[1] M. A. Syrunin,[1] L. A. Sobol',[2] A. V. Sukhanov,[2] and V. G. Popov[2]

UDC 624.074.4:678.067

The dynamic strength and deformability of basalt–plastic specimens under single pulsed (explosive) loading are studied experimentally. The results obtained show that the basalt–plastic specimens possess high specific strength and their strength characteristics are close to those of similar tubular specimens from glass-reinforced plastic based on a high-modulus glass fiber. It is found that a twofold increase in all geometrical dimensions of the specimens does not affect their specific carrying capacity.

One of the basic problems in developing explosion-resistant structures, in particular, explosion-protective containers, consists in choosing a material and parameters of the container pressure vessel. Ivanov and Fedorenko [1] showed that the most suitable material for the pressure vessel of an explosion-resistant container or chamber is a winding-type composite material based on a high-modulus glass fiber. At present, much attention is given to the problem of replacing the high-modulus glass fiber used as a material of the pressure vessel of explosion-protective containers by another material whose technical parameters are not worse than those of the glass fiber. As a substitute for the glass fiber, one can use a basalt fiber whose strength and elastic characteristics are close to those of the composite.

Table 1 summarizes experimentally obtained quasi-static physicomechanical characteristics of basalt plastic with unidirectional reinforcement based on an ÉDT-10 binder and roving from RB9-1200 basalt complex filaments (the diameter of an elementary filament is 9 μm) with a 4S oil. For comparison, the data for glass-reinforced plastic based on an RVMN 10-1260-80 roving and an ÉDT-10 binder are also listed in Table 1. Ring and plane unidirectional specimens were tested according to the standard methods of determining the corresponding physicomechanical characteristics. The mass fraction of the binder in the ring specimens of diameter 146–150 mm was 14.45–23.24% and that in the plane unidirectional specimens was 16.25–23.65%. In Table 1, we use the following notation: E_1 and E_2 are the tensile moduli of elasticity in the direction along and across reinforcement, respectively, E_{flex} is the flexural modulus of elasticity in the direction of reinforcement, σ_{1b} and σ_{2b} are the tensile rupture stresses along and across reinforcement, respectively, σ_{1b}^{-} and σ_{2b}^{-} are the compressive rupture stresses along and across reinforcement, respectively, σ_{bear}, σ_{trans}, and σ_{inter} are the bearing, transverse shear, and interlaminar shear stresses, respectively, G_{12} is the interlaminar shear modulus, $\varepsilon_{1\text{rupt}}$ and $\varepsilon_{2\text{rupt}}$ are the specific elongations at rupture in tension along and across reinforcement, respectively, and μ is Poisson's ratio. One can see from Table 1 that basalt plastic is as good as glass-reinforced plastic in terms of the basic quasi-static parameters of elasticity and strength characteristics.

The aim of the present work is to study experimentally the main characteristics of dynamic deformability and strength of basalt–plastic tubular specimens imitating the most loaded central zone of the pressure vessel of an explosion-resistant container under an internal explosive load.

Parameters of Tubular Specimens Tested. The geometrical dimensions and reinforcement parameters of shells made of the above-mentioned basalt plastic were as follows:

[1]Institute of Experimental Physics, Sarov 607190. [2]Institute of Mechanical Engineering, Moscow Region, Khot'kovo 141350. Translated from Prikladnaya Mekhanika i Tekhnicheskaya Fizika, Vol. 43, No. 1, pp. 186–195, January–February, 2002. Original article submitted May 3, 2001.

 0021-8944/02/4301-0154 $27.00

TABLE 1

Material	E_1	E_2	E_{flex}	σ_{1b}	σ_{2b}	σ_{1b}^-	σ_{2b}^-	σ_{bear}	σ_{trans}	σ_{inter}	G_{12}	$\varepsilon_{1\text{rupt}}$	$\varepsilon_{2\text{rupt}}$	μ
RB9-1200 + ÉDT-10	5184	1425	5160	112	4.88	64.2	13.0	12.0	20.0	4.14	574	2.18	0.34	—
	5483	1553	5586	131	5.98	95.0	16.3	19.9	26.7	4.99	618	2.93	0.39	—
	5356	1515	5347	121	5.55	84.4	14.8	16.1	22.2	4.69	590	2.40	0.37	0.290
RVMN 10-1260-80 + ÉDT-10	5500	904	—	150	2.67	39.7	7.19	14.0	21.8	3.57	508	2.33	—	0.276

Notes. 1. The quantities E_1, E_2, E_{flex}, σ_{1b}, σ_{2b}, σ_{1b}^-, σ_{2b}^-, σ_{bear}, σ_{trans}, σ_{inter}, and G_{12} are in kgf/mm^2 and $\varepsilon_{1\text{rupt}}$ and $\varepsilon_{2\text{rupt}}$ are in percent. 2. For all the parameters of the RB9-1200 + ÉDT-10 material except for Poisson's ratio μ, the minimum, maximum, and values averaged over a series of tests are given.

1) The inner diameter is $D = 150$ mm, the length is $L = 300$ mm, the thickness is $h = (6.6 \pm 0.2)$ mm, the angles of reinforcement relative to the generatrix are $\varphi \approx 90^\circ$ and $\varphi = \pm 35^\circ$, which correspond to alternating 7 double ring layers and 7 double spiral layers, and the average mass fraction of the binder is $(16.3 \pm 0.6)\%$;

2) $D = 295$ mm, $L = 600$ mm, $h = (13.5 \pm 0.5)$ mm, the angles of reinforcement relative to the generatrix are $\varphi \approx 90^\circ$ and $\varphi = \pm 35^\circ$, which correspond to alternating 14.5 double ring layers and 10 double spiral layers, and the average mass fraction of the binder is $(21.3 \pm 0.6)\%$.

The reinforcement parameters are similar to those that ensure high specific strength of cylindrical shells from a composite material based on a high-modulus glass fiber [2] under similar conditions of explosive loading.

basalt–plastic shell specimens were manufactured by wet winding around a cylindrical technological mandrel and subsequent thermal treatment, which was necessary to polymerize the binder.

Before tests, a steel shell of thickness $h_1 = 1$ and 2 mm was inserted into most of the specimens of the first and second types, respectively. The shells of the first type were manufactured by rolling a low-carbon steel sheet and its butt welding. In this case, the weld was of poorer quality and less plastic compared to the shells of the second type; therefore, cracks were formed along the weld in almost all tests. The shells of the second type were manufactured by rolling a thicker sheet and its butt welding and subsequent annealing and turning to prescribed dimensions. The outer diameter of the steel shell was chosen so as to ensure the minimum clearance relative to the inner diameter of the basalt–plastic shell. According to the results of testing glass-reinforced plastic shells [3], the use of a two-layered structure of the pressure vessel increases the specific explosion strength.

Statement of Tests. Figure 1 shows a diagram of the experimental setup. To record the main parameter, i.e., the circumferential strain ε_1 in the cross section where a high-explosive (HE) charge is located, we used circumferential strain gauges from a nichrome wire with bifilar winding along the entire length of the circumference [4]. The radial expansion of the shell in the central cross section ΔR_{out} was measured by high-speed slot photographic recording [5]; based on this quantity, the circumferential axisymmetric strain was determined. To measure the longitudinal strains in the central cross section ε_3, we used industrial strain gauges KF-5, which allow one to record strains up to 3–5%. The error in determining the maximum value of the parameter measured was smaller than 10%.

To determine the parameter of the specific explosive load $\xi = M_{\text{HE}}/M$, where M_{HE} is the mass of the HE charge and $M = M_1 + M_2$ is the total mass of the steel shell (M_2) and basalt–plastic shell (M_1), the charge and shells were weighed with an error of 1% or smaller. To determine the circumference strain $\varepsilon_1 = \Delta R_{\text{out}}/R_{\text{out}}$ from the results of slot photographic recording of radial expansion of the shell ΔR_{out}, we measured the outer diameter of the shell $D = 2R_{\text{out}}$ in different cross sections near its both ends with an error of approximately 0.1% and calculated the outer radius R_{out} for the averaged value of D.

Each specimen was subjected to explosive loading once (only in one case, an undamaged shell was loaded repeatedly). During the tests, the ambient temperature was 10–25°C.

Experimental Results. The following quantities were determined from the experimental results: the maximum circumferential tensile strain in the central cross section ε_1 and the time of its occurrence τ_1, the maximum circumferential compressive strain in the central cross section ε_2, the maximum longitudinal strain in the central cross section ε_3, the period of the fundamental tone of radial oscillations T, and the maximum circumferential strain rate $\max(d\varepsilon_1/d\tau)$. The character of damages of a specimen was studied and their dimensions were measured.

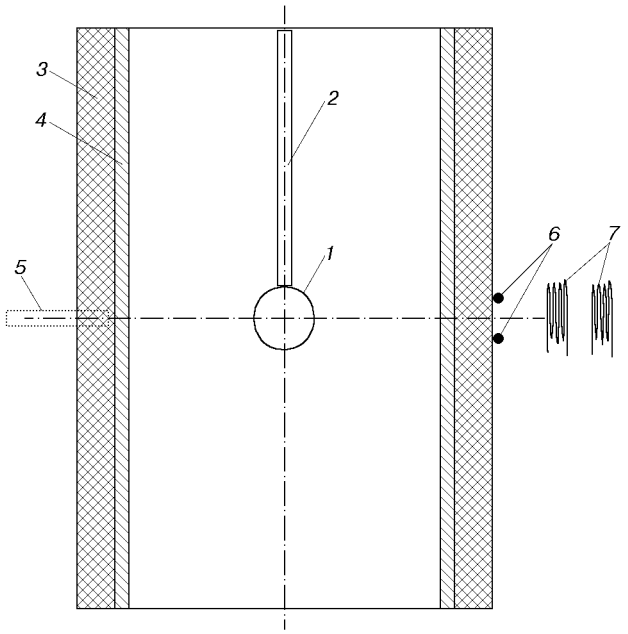

Fig. 1. Diagram of the experimental setup: 1) HE charge from a 50/50 TNT/RDX alloy; 2) rod for HE suspension; 3) basalt–plastic shell; 4) steel shell; 5) region of the high-speed slot photographic recording of radial expansion of the shell; 6) circumferential strain gauges with a base $2\pi R$; 7) longitudinal strain KF-5 gauges with a base of 20 mm.

TABLE 2

Test No.	Specimen No.	h, mm	R_{out}, mm	h_1, mm	M, g	M_{HE}, g	$\xi \cdot 10^3$	ε_1, %	τ_1, μsec	ε_2, %	ε_3, %	T, μsec	$\max(d\varepsilon_1/d\tau)$, sec^{-1}
1	1	6.70	81.70	—	2054	23.80	11.59	2.20	45.1	−1.1	—	123	597
2	2	6.80	81.80	—	2060	37.40	18.16	2.45	34.6	−1.5	0.30	—	856
3	3	6.60	81.60	1	2980	46.00	15.64	2.90	43.2	−1.4	1.85	112	891
4[1]	3	6.60	81.60	1	2980	62.20	21.15	3.70	43.3	—	—	—	1188
5	4	6.70	81.70	1	3101	59.70	19.51	—	—	—	—	—	—
6	5	6.80	81.80	1	3057	90.70	30.07	4.70	41.7	—	—	—	1498
7	6	6.80	81.80	1	3125	81.15	26.32	4.35	49.8	—	2.10	—	919
8	7	6.77	81.77	1	3120	69.17	22.47	3.80	44.7	—	—	—	847
9	8	6.77	81.77	1	3070	63.00	20.61	3.20	43.2	−0.9	—	—	978
10	9	6.79	81.80	1	3135	30.10	9.63	1.72	42.1	−0.86	—	121	592

[1]Results of repeated loading.

TABLE 3

Test No.	Specimen No.	h, mm	R_{out}, mm	h_1, mm	M, g	M_{HE}, g	$\xi \cdot 10^3$	ε_1, %	τ_1, μsec	ε_2, %	T, μsec	$\max(d\varepsilon_1/d\tau)$, sec^{-1}
1	1	13.47	161.22	—	15,750	135.0	8.70	1.47	75.0	−0.86	245	234
2	2	13.17	160.75	2.17	24,750	633.0	26.38	4.80	100.0	—	—	613
3	3	13.75	161.70	2.10	24,990	484.6	19.94	3.60	94.8	−1.60	—	507

The initial parameters of specimens and the measurement results for shells of the first and second types are listed in Tables 2 and 3, respectively. For a correct comparison with the existing data on glass-reinforced plastics, the values of the specific explosive load $\xi = M_{\text{HE}}/M'$ [$M' = 4M(R_{\text{out}} - h - h_1)/L$ is the mass of the two-layered shell whose length is equal to four inner radii] are given in Tables 2 and 3. If a quantity was measured repeatedly in a test, its averaged value is given.

Below, we describe the state of a tested shell.

1. The shell does not fail. Peeling of the material of thickness 1.2 mm occurs at the inner surface (test No. 1 in Table 2).

2. A through hole 7 mm in diameter is formed in the shell; thicknesses of the peeled material are 3 and 1 mm at the inner and outer surfaces, respectively (test No. 2 in Table 2).

3. The shell does not fail; the steel layer buckles in the neighborhood of the weld (a dent 40 mm wide and 10 mm deep is formed; near the lower end of the shell, the welded edges move apart for a length of 50 mm (test No. 3 in Table 2).

4. The shell is at the initial stage of fracture; a damage 45 mm wide and 0.7 mm deep occurs at the outer layer reinforced in the circumferential direction, the layer with spiral winding is loosened, and the steel layer is torn apart over a length of 35 mm (test No. 4 in Table 2).

5. The shell does not fail; peeling of the material of width of 8 mm and thickness of 0.5 mm occurs at the outer surface; the steel layer buckles (test No. 5 in Table 2).

6. The shell fails at the first stage of expansion; the residual strain in the central part of the shell 31 mm wide is 35% (test No. 6 in Table 2).

7. The shell is at the stage of fracture; three bands 60 mm wide are peeled; the residual strain is 7.2%; in the steel layer, a crack is formed along the weld (test No. 7 in Table 2).

8. The shell does not fail; a band 45 mm wide and 0.6 mm thick is peeled; the steel layer buckles, and a 35-mm crack is formed along the weld (test No. 8 in Table 2).

9. Several filaments peel from the shell; the steel weld is at the initial stage of buckling, and a 280-mm crack is formed along the weld (test No. 9 in Table 2).

10. The shell does not fail (test No. 10 in Table 2; test No. 1 in Table 3).

11. The shell fails at the first stage of expansion; the layers reinforced in the circumferential direction fail, and the layers with spiral winding are loosened; the residual strain in the central cross section is approximately 17%; the steel layer does not fail (test No. 2 in Table 3).

12. The shell is at the initial stage of fracture; two or three outer layers 35 mm wide fail; the steel layer buckles but does not fail (test No. 3 in Table 3).

Figure 2 shows the results of high-speed photographic recording of the dynamic response of the specimen to explosive loading in the absence of fracture, for fracture after the initial stage of compression, and at the first stage of expansion.

Figure 3 shows the photographs of specimens of the first and second types with different degrees of damage.

Discussion and Analysis of Results. Figure 4 shows the dependences $\varepsilon_1(\xi)$ for the tested shells of both types. The dark points refer to failed shells, gray points refer to shells with surface damages, and light points refer to nonfailed and almost damage-free shells. One can see from Fig. 4 that, within the limits of the measurement error, these dependences are linear and very close to each other.

Figure 4 also shows the experimental dependences of the circumferential strain ε_1 on the specific explosive load ξ obtained in [2, 6] for similar glass-reinforced plastic specimens with similar reinforcement parameters. A comparative analysis of these dependences shows that, under dynamic loading, basalt–plastic shells behave like glass-reinforced plastic shells, i.e., shells from a linear-elastic material, up to the failure (see [2, 3, 6]). However, for basalt–plastic shells of the second type, the slope of the curve $\varepsilon_1(\xi)$ for a smaller angle of spiral reinforcement is smaller than the slope of the corresponding curve for similar glass-reinforced plastic shells by approximately 9%. Thus, the basalt–plastic shells are stiffer since they have more layers reinforced in the circumferential direction.

Limiting Deformability and Specific Strength of basalt–plastic Shells. One can see from Table 2 (test Nos. 1 and 2) that, in the absence of a stiffening steel layer, the rupture circumferential strain of basalt–plastic specimens 150 mm in diameter is 2.2–2.45%, which is almost 25% smaller than for glass-reinforced plastic specimens whose reinforcement parameters are closest to those considered in [6], where the range of the ultimate strains was determined to be 3.1–3.3%. As in the case of glass-reinforced plastic shells [2, 3, 6], the ultimate strain and specific strength of a basalt–plastic shell increase significantly if a steel shell is inserted into it. For example, the ultimate strain and specific strength of basalt–plastic specimens of the first (or second) type reinforced by a steel layer lie within the ranges $\varepsilon_1 = 3.7$–4.35% (or $\varepsilon_1 = 3.6$–4.8%) and $\xi = 21.2 \cdot 10^{-3}$–$26.3 \cdot 10^{-3}$ (or $\xi = 19.9 \cdot 10^{-3}$–$26.4 \cdot 10^{-3}$), respectively. According to [6], for glass-reinforced plastic shells with a steel layer of thickness equal to approximately 20% of the composite thickness, we have $\varepsilon_1 = 3.9$–5.0% and $\xi = 18.9 \cdot 10^{-3}$–$22.7 \cdot 10^{-3}$. It is noteworthy that, as in the case of glass-reinforced plastic, the ultimate strains of basalt plastic increase to 4.35–4.8% (see Tables 2

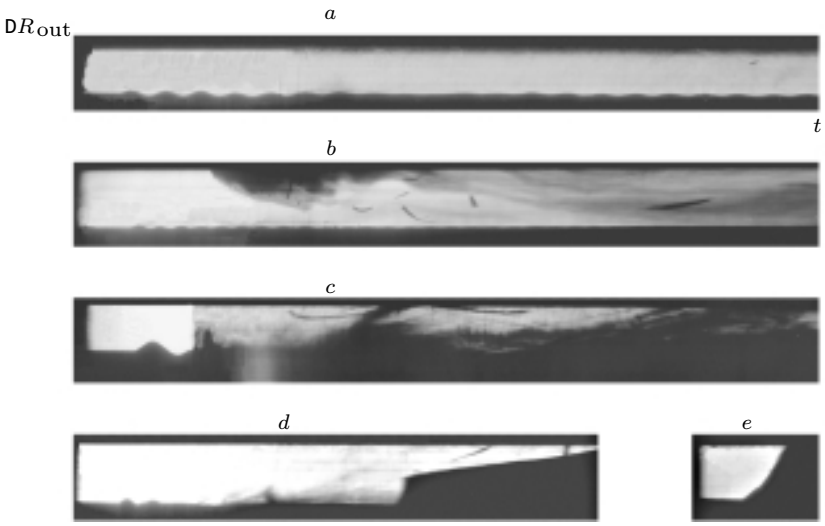

Fig. 2. Shade streak photography of radial expansion of a shell for different levels of loading: (a) oscillations of a nonfailed shell without a steel layer (test No. 1 in Table 3); (b) oscillations of a nonfailed shell with a steel layer (test No. 10 in Table 2); (c) fracture after the stage of compression (test No. 3 in Table 3); (d) fracture as a result of peeling (test No. 9 in Table 2); (e) fracture at the first stage of expansion (test No. 2 in Table 3).

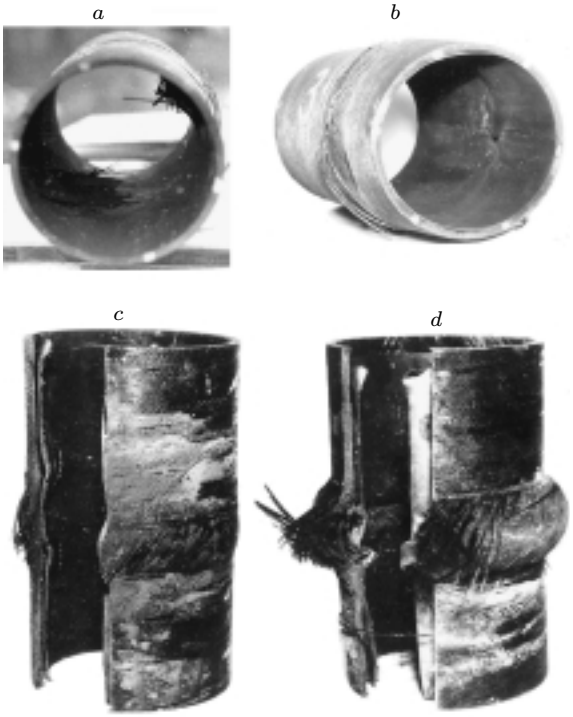

Fig. 3. Appearance of a shell after test Nos. 2 (a), 4 (b), 7 (c), and 6 (d) (see Table 2).

and 3) at the initial stage of expansion for dynamic fracture. This value is nearly twice as high as the ultimate strain of unidirectionally reinforced basalt–plastic specimens under quasi-static extension, which is equal to 2.4% (see Table 1).

It follows from the data considered above basalt–plastic shells possess high specific strength close to that of glass-reinforced plastic shells. A comparative analysis of the data for the specimens of the first and second types

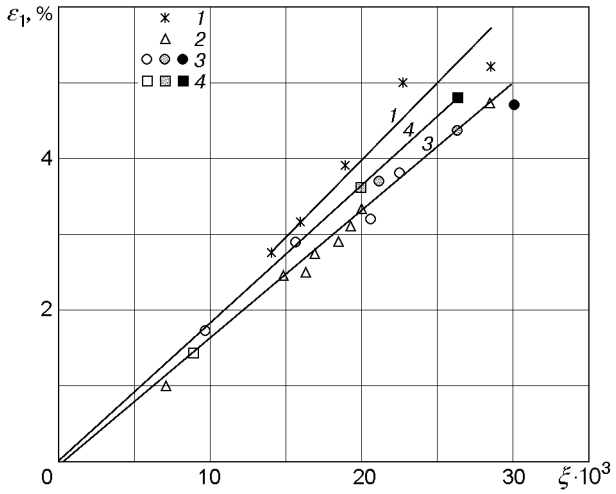

Fig. 4. Experimental dependences of the maximum circumferential strain ε_1 on the specific explosive load ξ: points 1 refer to the data of [6] for glass-reinforced plastic shells with an inner steel layer of thickness $h_1 = 2$ mm [the inner radius is $R = 150$ mm, the length is $L = 4R$, and the relative wall thickness is $h/R = 4.8$–7%, alternation of the spiral ($\varphi_1 = \pm 45^\circ$) and ring ($\varphi_2 = 90^\circ$) layers (the thickness ratio is $k = 1 : 1$)], points 2 refer to the data of [2] for glass-reinforced plastic shells without an inner steel layer [$2R = 300$–320 mm, $L = 600$ mm, $h/R = (8 \pm 2.9)\%$, $\varphi_1 = \pm 45^\circ$, $\varphi_2 = 90^\circ$, and $k = 1 : 1$], points 3 refer to basalt–plastic specimens of the first type with an inner steel layer (diameter 150 mm), and points 4 refer to basalt–plastic specimens of the second type with an inner steel layer (diameter 295 mm) (the open square refers to a basalt–plastic specimen without an inner steel layer); curves 1, 3, and 4 are linear approximations of the corresponding experimental dependences.

(i.e., for specimens of different dimensions) shows that the characteristics of limiting deformability and specific strength of basalt–plastic shells remain unchanged as their dimensions increase twofold (i.e., as the maximum strain rate of large specimens decreases compared to small specimens from 1000 to 500 $\sec^{-1}$).

Estimation of Elastic Constants of Basalt Plastic from the Data of Dynamic Tests. Similarly to [2], the elastic constants of reinforced tubular basalt–plastic specimens can be estimated from the elastic constants of the binder and fiber by the method proposed in [7].

Calculations were performed for the following physicomechanical characteristics of the ÉDT binder [8]: Young's modulus $E_{\text{bind}} = 2.9 \cdot 10^3$ MPa, Poisson's ratio $\mu_{\text{bind}} = 0.4$, and density $\rho_{\text{bind}} = 1230$ kg/m^3. The volume fraction of the binder θ_{bind} can be calculated by the formula $\theta_{\text{bind}} = \rho\theta/\rho_{\text{bind}}$, where $\rho = 2060$ kg/m^3 is the density of the specimens and $\theta = 0.1527$ is the mass fraction of the binder. The modulus of elasticity and density of basalt fiber, which are necessary for the calculations, are unknown. It follows from the data of [9] that natural basalt is characterized by a wide scatter of data on its chemical composition and physicomechanical properties. For example, its modulus of elasticity, Poisson's ratio, and density may vary within the limits $E_{\text{basalt}} = 6.2$–$11 \cdot 10^{10}$ Pa, $\mu_{\text{basalt}} = 0.2$–$0.25$, and $\rho_{\text{basalt}} = 2520$–$2970$ kg/m^3, respectively. Therefore, we confine ourselves to estimation of lacking characteristics of basalt fibers from the data available.

Using the additivity law [8] $E_1 = E_{\text{fiber}}(1 - \theta_{\text{bind}}) + E_{\text{bind}}\theta_{\text{bind}}$ [$E_1 = 5.254 \cdot 10^{10}$ Pa is the average value of the modulus of elasticity of the unidirectionally reinforced basalt–plastic specimen (see Table 1)], we obtain the modulus of elasticity of basalt fiber $E_{\text{fiber}} = 6.96 \cdot 10^{10}$ Pa. From the equation $\rho = (1 - \theta_{\text{bind}})\rho_{\text{basalt}} + \theta_{\text{bind}}\rho_{\text{bind}}$, we find its density: $\rho_{\text{basalt}} = 2345$ kg/m^3. These characteristics of basalt fiber are close to the lower bound of the reference data for natural basalts. Poisson's ratio was taken to be $\mu_{\text{basalt}} = 0.225$, which is the average value for natural basalts [9].

In basalt–plastic specimens of both types, the layers with different winding angles φ are characterized by the relative thickness δ (i.e., ratio of the thickness of the layers with a given winding angle to the total thickness of the packet). For the first type, $\delta = 0.5$ at $\varphi = \pm 35^\circ$ and $\varphi = 90^\circ$, and for the second type, $\delta = 10 : 25.5$ at

TABLE 4

Specimen type	E_y, GPa	E_x, GPa	G_{xy}, GPa	μ_{xy}	μ_{yx}
First	36.05	24.52	10.94	0.140	0.206
Second	33.44	19.50	8.81	0.119	0.204

$\varphi = \pm 35^\circ$ and $\delta = 14.5 : 25.5$ for $\varphi = 90^\circ$. The mass fractions of the binder are 16.3 and 21.3% for the first and second types, respectively. The axial (E_x) and circumferential (E_y) moduli of elasticity of the basalt–plastic packet and Poisson's ratios calculated in [7] for these orthotropic materials are listed in Table 4.

The fundamental frequency of radial oscillations of a free cylindrical shell can be determined from the relation given in [10], which can be rewritten in the form

$$f' = \frac{1}{2\pi R_{\rm m}} \sqrt{\frac{E_y - E_x \mu_{yx}^2}{\rho(1 - \mu_{xy}\mu_{yx})}},$$

where $R_{\rm m} = R_{\rm out} - h/2$ is the middle radius of the shell and μ_{xy} and μ_{yx} are Poisson's ratios.

For both types of basalt plastic, the periods of the fundamental tone of radial oscillations of the shell without a steel layer $T' = 1/f'$ calculated for quasi-static elastic characteristics ($T_1' = 117$ μsec and $T_2' = 234$ μsec) agree well (discrepancy does not exceed 5%) with the average experimental values of T ($T_1 = 123$ μsec and $T_2 = 245$ μsec) (see test No. 1 in Tables 2 and 3). These results show that dynamic loading has little effect on the elastic characteristics of wound basalt plastic, which agrees with the conclusion obtained in [2, 6] for glass-reinforced plastic.

Specific Features of Fracture and Damage of Basalt–Plastic Shells. During tests of basalt–plastic shells under explosive loading, the following specific features of the dynamic response, damage, and fracture were revealed.

For relatively low explosive loads that do not cause any visible damages, the dynamic response of basalt–plastic shells is characterized by damping oscillations of the beating type with the dominant fundamental frequency of radial oscillations of the shell without a steel layer (see Fig. 2a). The response of the shell with a steel layer is similar. In this case, however, beating is absent (see Fig. 2b) owing to a higher damping factor for plastic strains of steel and contact friction between steel and basalt plastic. Similar specific features of the dynamic response are also characteristic of glass-reinforced plastic shells [3, 6].

Like glass-reinforced plastic shells, basalt–plastic shells without a stiffening steel layer fail after the first stage of compression for a relatively small maximum circumferential strain (approximately 2.5%). The failure occurs as a result of flexural modes of motion of the central zone (see Figs. 2c and 3a). In this case, the material of the shell buckles both inward and outward (see Fig. 3a).

For a shell reinforced by a steel layer, slight damages in the form of peeling of one or two outer layers (see Fig. 3b) occur for a maximum circumferential strain of 3.2–3.8%. The dynamics of peeling is shown in Fig. 2d. One can see that peeling begins after the radial expansion of the shell reaches a maximum.

A further increase in the explosive load leads to the failure of the circumferential layers at the first stage of expansion (see Figs. 2e and 3c and d). The strain recorded at the inflection point of the curve $\varepsilon_1(\xi)$ (see Fig. 2e) may be considered as the ultimate strain of the ring layers under dynamic extension with a high initial strain rate (500–1000 sec^{-1}). At the same time, the spiral fibers are less stressed and do not fail despite the failure of the binder (see Fig. 3d and e). In this case, a ring fracture zone is characterized by spiral layers freed of the binder, where the failed packet of the basalt–plastic layer buckles outward. The steel layer in this region undergoes considerable flexural and circumferential strains and also can fail (see Fig. 3c and d).

As a whole, the behavior (in particular, the multistage character of damage accumulation and fracture) of basalt–plastic and glass-reinforced plastic shells under dynamic loading is similar.

An analysis of the data obtained shows that loading of basalt–plastic shells reinforced by a steel layer to circumferential strains of approximately 3.5% does not lead to inadmissible damage of ring layers of basalt plastic (loss of working capacity). This suggests that the closed shells of the pressure vessel of explosion-protective containers can sustain a sufficiently high gas pressure that acts after the pulsed explosive loading. Thus, a strain of approximately 3.5% may be considered as the limiting safe strain for basalt plastic that enters into the composition of tubular specimens with a steel layer. Under similar conditions, the ultimate strain of glass-reinforced plastic tubular specimens with a steel layer is approximately 3.3% [6]; for closed cylindrical shells with hemispherical bottoms, its value decreases very slightly and is equal to 3.1–3.5% [1].

For a higher load that causes a specimen to fail at the first stage of expansion, the dynamic rupture strain of basalt plastic is 4.4–4.8%, which is close to a value of 4–5% determined for tubular specimens and closed models of containers [1, 2, 6]. This value can be interpreted as the ultimate strain of unidirectional (ring) layers of the packet under dynamic extension with a strain rate of 500–1000 $\sec^{-1}$. As in the case of glass-reinforced plastic, it is nearly twice as high as its static ultimate strain.

The explosion tests performed on tubular basalt–plastic specimens lead to the following conclusions.

1. The dynamic response of the shells to nondestructive loads is similar to the response of glass-reinforced plastic shells with similar reinforcement parameters, provided the elastic properties of the material determined in static tests remain unchanged under dynamic conditions.

2. The dynamic ultimate strain and specific strength of basalt–plastic tubes under internal explosive loading are not smaller than those for glass-reinforced plastic shells. These quantities remain unchanged as the specimen dimensions increase twofold.

3. The composite material considered can be used in structures of load-bearing shells of explosion-protective containers.

REFERENCES

1. A. G. Ivanov and A. G. Fedorenko, "Utility of the use of composite materials for a protective shell of a nuclear power station," *Atom. Énerg.*, **75**, No. 1, 45–48 (1993).
2. A. G. Fedorenko, M. A. Syrunin, and A. G. Ivanov, "Effect of the reinforcement structure of oriented glass-reinforcement plastics on the strength of circular cylindrical shells for internal explosive loading," *Mekh. Kompoz. Mater.*, No. 4, 631–640 (1991).
3. V. I. Tsypkin, V. N. Rusak, A. G. Ivanov, et al., "Deformation and fracture of two-layered metal–plastic shells under internal pulsed loading," *Mekh. Kompoz. Mater.*, No. 5, 833–838 (1987).
4. A. T. Shitov, V. N. Mineev, O. A. Kleshchevnikov, et al., "Wire transducer for continuous recording of large strains of structures under dynamic loading," *Fiz. Goreniya Vzryva*, No. 2, 304–307 (1976).
5. A. S. Dubovik, *Photographic Recording of Fast Processes* [in Russian], Nauka, Moscow (1975).
6. A. G. Ivanov, M. A. Syrunin, and A. G. Fedorenko, "Effect of reinforcing structures on the critical deformability and strength of shells made of oriented glass-plastic composites under an internal explosive load," *Prikl. Mekh. Tekh. Fiz.*, No. 4, 130–135 (1992).
7. *Proceedings of Central Aerohydrodynamic Institute*, No. 1: *Design, Calculation, and Tests of Structures from Composite Materials* [in Russian], Moscow (1973), p. 143.
8. G. M. Gunyaev, *Structure and Properties of Polymeric Fiber Composites* [in Russian], Khimiya, Moscow (1981).
9. E. A. Kozlovskii (ed.), *Mining Encyclopedia* [in Russian], Vol. 1, Sov. Éntsiklopediya, Moscow (1984).
10. V. L. Bazhanov, I. I. Gol'denblat, V. A. Kopnov, et al., *Strength of Glass-Reinforced Plastics* [in Russian], Mashinostroenie, Moscow (1968).